Vacuum 121 (2015) 294–299

Contents lists available at ScienceDirect

Vacuum

journal homepage: www.elsevier.com/locate/vacuum

Effect of pulse phase lag in the dual synchronized pulsed capacitive coupled plasma on the etch characteristics of SiO_2 by using a $C_4F_8/Ar/O_2$ gas mixture

Min Hwan Jeon [a], Kyung Chae Yang [b], Kyong Nam Kim [b], Geun Young Yeom [a, b, *]

[a] SKKU Advanced Institute of Nanotechnology(SAINT), Sungkyunkwan University, Suwon, Kyunggi-do, 440-746, South Korea
[b] Department of Advanced Materials Science and Engineering, Sungkyunkwan University, Suwon, Kyunggi-do, 440-746, South Korea

ARTICLE INFO

Article history:
Received 13 October 2014
Received in revised form
11 May 2015
Accepted 12 May 2015
Available online 22 May 2015

Keywords:
Synchronous pulse plasma
Pulsed dual frequency CCP
SiO_2 etching

ABSTRACT

The characteristics of a synchronized pulse plasma using 60 MHz radio frequency as a source power and 2 MHz radio frequency as a bias power were investigated for the etching of SiO_2 masked with an amorphous carbon layer (ACL) in a $C_4F_8/Ar/O_2$ gas mixture. Especially, the effects of the pulse phase lag of the synchronized dual-frequency pulsing between source power and bias power on the characteristics of the plasma and SiO_2 etching were investigated. The results showed that the etch rates of SiO_2 was the highest and the etch profile was the most anisotropic when the pulse phase lag between the source power and bias power was 0° in the synchronized pulse plasma. Increasing the phase lag to 180° decreased the etch rates and degraded the etch anisotropy. The change in etch characteristics as a function of pulse phase lag was believed to be related to the difference in gas dissociation and fluorocarbon passivation caused by the variations in electron temperatures during the source pulse off-time.

1. Introduction

As the size of semiconductor devices decreases to the deep nanoscale, the dry etch process, which has a higher aspect ratio, a higher etch selectivity, tighter critical dimensional control, and lower plasma induced damage is required more significantly [1–5]. Currently, it is difficult to etch high aspect ratio contact (HARC) holes with good etch uniformity and decent etch profiles without plasma induced damage on the contact hole when etching nano-sized contact holes using conventional continuous wave (CW) plasmas. This is because several issues such as etch stop, reactive ion etching (RIE) lag, pattern distortion, and charging damages occur while etching the HARC pattern using conventional plasma etching processes [6–10].

Therefore, various plasma etching methods have been widely investigated to control critical plasma properties for low damage nanoscale etching. Pulsed plasma techniques that turn the plasma on and off with a frequency of a few kHz during the etching is one of the most promising candidates for the improvement of etch characteristics in the etching of nanoscale semiconductor materials. By adjusting pulse parameters such as the duty ratio and the pulse frequency of the pulsing during the operation of the plasmas, additional and independent control of plasma characteristics such as plasma chemical composition and ion bombardment energy is possible. The reported main advantages of the pulsed plasma are the improvement of etch selectivity and etch uniformity due to decreased gas dissociation and enhanced radical diffusion. Also, control of the etch profile and critical dimensions was reported due to the reduction of plasma induced damages such as charge build up damage by the electron shading effect during the pulse off period. Thus, pulsed plasma technology is widely investigated for nanoscale etching applications to improve plasma uniformity, etch selectivity, and etch profile by reducing plasma induced damages [11–16].

Even though pulsed plasmas have been widely studied, due to the significant range of pulsing variables, the relationship between the etch properties and the pulsed plasma is still not clear and needs to be investigated in more detail. Especially, due to the complexity of the gas phase chemical reactions for carbon-rich fluorocarbon-based gases, it is more difficult to understand the precise etching mechanism in the pulsed plasmas used in HARC etching.

In this study, a synchronously pulsed dual-frequency capacitive coupled plasma (DF-CCP) composed of a pulsed 60 MHz power on

* Corresponding author. Department of Advanced Materials Science and Engineering, Sungkyunkwan University, Suwon, Kyunggi-do, 440-746, South Korea.
E-mail address: gyyeom@skku.edu (G.Y. Yeom).

http://dx.doi.org/10.1016/j.vacuum.2015.05.009
0042-207X/

the top electrode as the source power and a pulsed 2 MHz power on the bottom electrode as the bias power to the substrate was used with a $C_4F_8/Ar/O_2$ gas mixture for the highly anisotropic etching of nanoscale SiO_2 contact. Especially, the effect of the pulse phase lag between the source power and the bias power on the plasma characteristics and the etching characteristics was investigated to study the effect of synchronized pulsing using a dual pulsed plasma on the etch characteristics of HARC.

2. Experiment

The experimental setup for the synchronized pulse DF-CCP system used in this study is shown in Fig. 1. The rf discharge was maintained between two parallel plate electrodes separated by 30 mm. The top electrode was covered with a perforated silicon plate to flow gases uniformly and was connected to a 60 MHz rf power (high frequency; HF) source which could be pulsed to control the plasma characteristics and to control the pulse signal delay of the 2 MHz (low frequency; LF) pulsed rf power applied to the substrate. The synchronization of 2 MHz rf power to 60 MHz rf power was achieved by connecting the 60 MHz pulse signal to the digital delay generator (DDG 645, SRS), to the signal generator (8657B, HP), and to the rf power amplifier (A1000, ENI) in series. Therefore, the source power pulse served as a master and the bias power pulse served as a slave by receiving the source pulse signal from the DDG. The reactor was evacuated by turbo molecular pumps (3200 *l*/s) backed by a dry pump. The gas was equally distributed through a baffle system from the top electrode. The pulse signal generated from the 60 MHz was also used to control the time-resolved optical emission spectrometer (OES) installed in the process chamber.

The 2 μm thick SiO_2 deposited on silicon wafers was masked with a 600 nm thick amorphous carbon layer (ACL). The ACL was used as the hardmask for SiO_2 HARC etching to maintain the critical dimension (CD) of the contact hole. The SiO_2 layer was etched for various pulse parameters during synchronized pulsing with a $C_4F_8/Ar/O_2$ gas mixture (60 MHz HF power/2 MHz bias voltage = 300 W/- 900 V, $C_4F_8/Ar/O_2$ = 40/155/5 sccm, and a process pressure of 26.6 mbar) while keeping the substrate temperature at room temperature.

Etch characteristic such as the etch rate of SiO_2 HARC layer/ACL and the etch profiles using the $C_4F_8/Ar/O_2$ gas mixture were estimated by field emission scanning electron microscopy (FE-SEM, Hitachi S-4700). The radicals that dominantly affected the etching were observed using time-resolved OES. The time-resolved OES (Andor istar 734) was performed with a spectrometer composed of a grating monochromator and an intensified charge coupled device (ICCD). For the time-resolved data collection, the OES data were collected with the interval of 100 μs in 1 kHz of pulse period and the data were averaged after 10 collections. The instant change in the electron temperature for the synchronized pulse conditions of 60/2 MHz DF-CCP was calculated using a home-made emissive probe. Also, the chemical binding characteristics of the etched SiO_2 surface for the differently synchronized pulse conditions were observed using X-ray photoelectron spectroscopy (XPS, ESCA2000, VG Microtech Inc.).

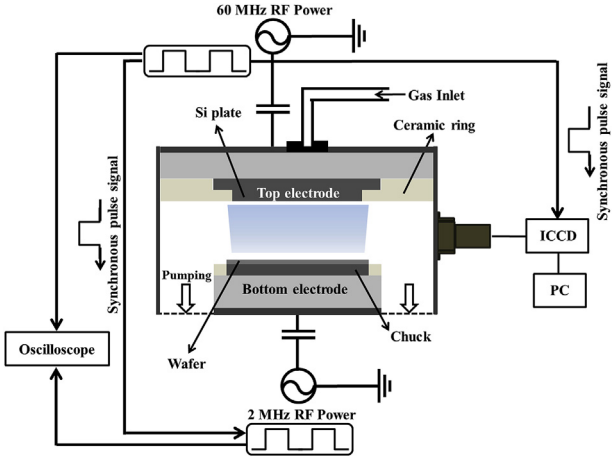

Fig. 1. Schematic diagram of the synchronized pulse dual-frequency CCP. A Pulsed 60 MHz source pulse power was applied to the top electrode to control the plasma characteristics and a pulsed 2 MHz bias power was applied to the bottom electrode to control the ion energy to the substrate.

3. Results and discussion

While pulsing with only the 60 MHz source power without the 2 MHz bias power in the $C_4F_8/Ar/O_2$ gas mixture, the plasma density decreased exponentially when the rf power was turned off during the pulse-off time, due to the lack of rf power to the plasma. The gas molecules and atoms dissociated in the plasma during the pulse on-time, as CF_x and F tend to recombine. In our study, in addition to the 60 MHz source power, the 2 MHz bias power applied to the substrate was synchronously pulsed with the source power and the effect of the pulse phase lag between the source rf power pulsing and the 2 MHz bias power pulsing on the plasma characteristics was investigated. Fig. 2 shows a cartoon figure of the synchronized pulse waveform for the pulse phase lags between the source power pulsing and the bias power pulsing during the synchronously pulsed 60/2 MHz CCP. As shown in the figure, the phase lag of the bias power pulse to the source power pulse was varied from 0° to 180°.

Fig. 3 shows the time-resolved optical emission intensity ratios for F/Ar, CF_2/Ar, CF_3/Ar, and CF_2/Ar measured as a function of pulse

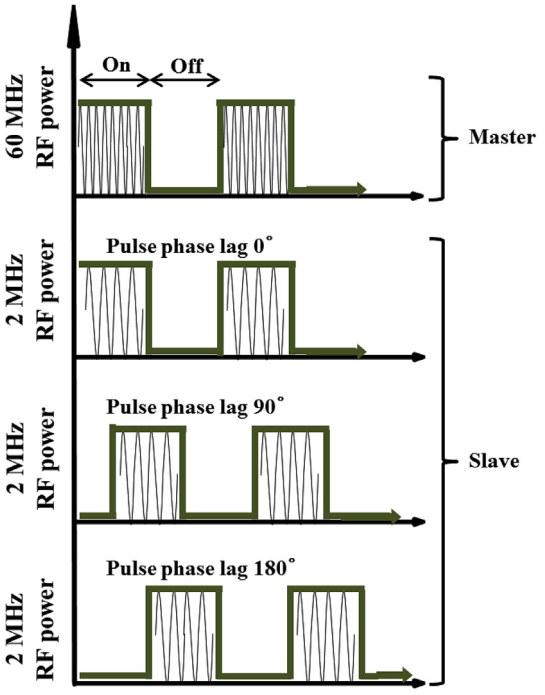

Fig. 2. Schematic diagram of pulse waveform between the source power pulsing and the bias power pulsing for various pulse phase lags in the synchronized pulse 60/2 MHz CCP.

phase lag from 0° to 180° for the DF-CCP using a $C_4F_8/Ar/O_2$ gas mixture. As the optical emission peak intensities, the peak intensities observed at 703 nm, 245–265 nm, 265–285 nm, and 751 nm were used for F, CF_2, CF_3, and Ar, respectively. The optical emission intensity ratios of the dissociated radicals to Ar were used to estimate the radical concentration in the plasma. For the time-resolved OES, 300 W of 60 MHz rf power and −900 V of 2 MHz rf voltage were used with the gas flow rates of $C_4F_8/Ar/O_2 = 50/145/5$ sccm and at 26.6 mbar of operating pressure. The pulse duty ratio and the pulse frequency were kept at 50% and 1 kHz, respectively. The OES data for the CW power condition of both the source power and the bias power (that is, 60 MHz CW source power/2 MHz CW bias power) is also included as references in Fig. 3(a). As shown in Fig. 3(a), when the source power and the bias power were not pulsed, the radical concentrations of CF_x(x = 2, 3) and F remained similar without variations in the time. However, when both the source and bias power were pulsed together with the pulse phase lag of 0° as shown in Fig. 3(b), the radical densities and the ratios of CF_x (x = 2, 3)/F during the pulse on-time (0–500 μs) for both power sources were similar to those observed when both powers were turned on in Fig. 3 (a). However, during the initial source power off-time (500–600 μs), F radicals decreased more rapidly than other radicals such as CF_2 and CF_3. Therefore, the ratios of CF_x (x = 2,3)/F increased during the initial source power pulse off-time, indicating enhanced recombination of the dissociated gas mixtures. The ratio remained similar during the rest of the pulse-off time (600–1000 μs).

When the source power and the bias power were pulsed with the pulse phase lag of 90° during the initial source power on-time of 0–250 μs, only 60 MHz rf power was applied to the source,

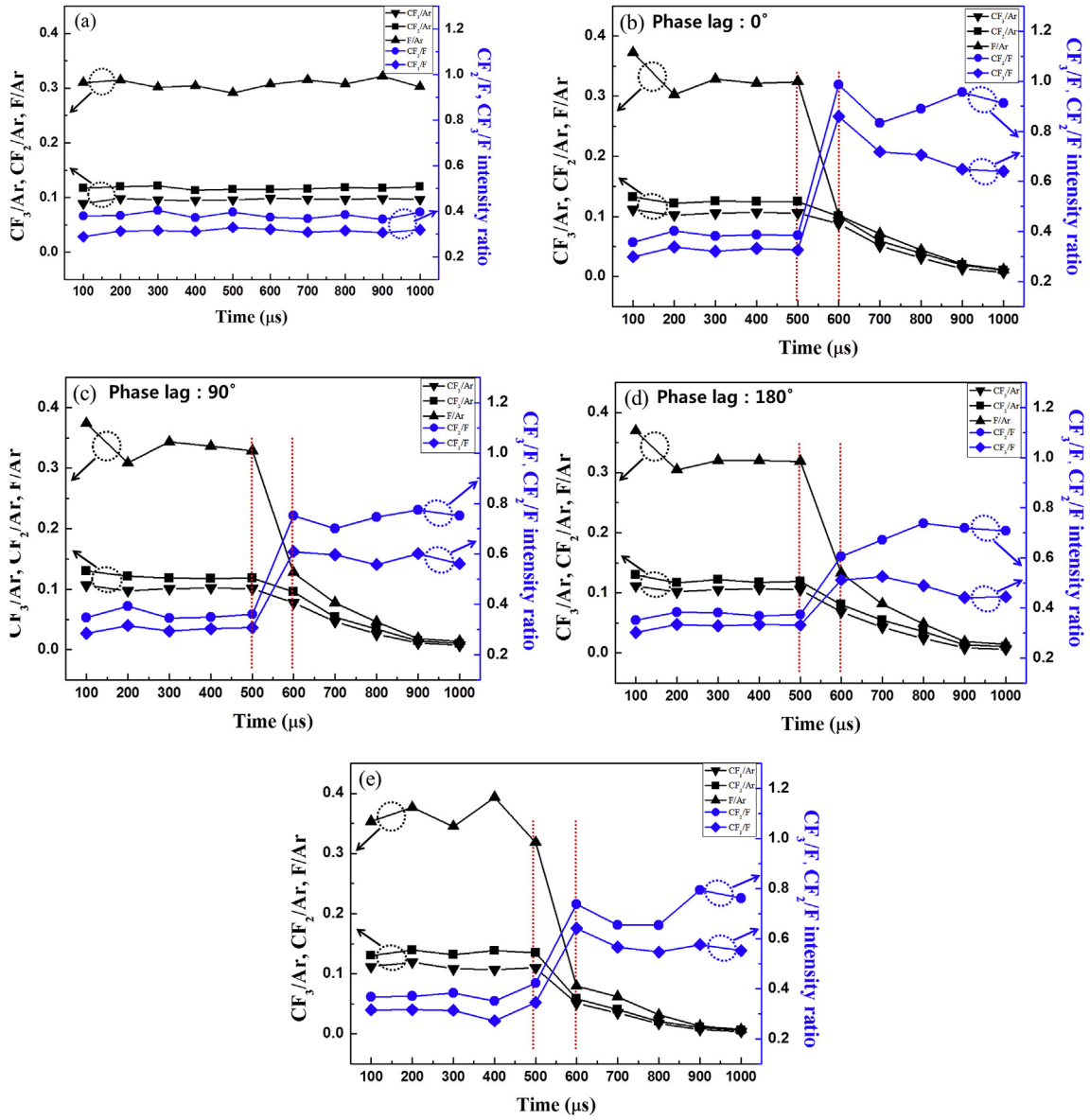

Fig. 3. Optical emission intensity ratios of CF_x(x = 2,3)/F, F/Ar, and CF_x (x = 2,3)/F in the synchronously pulsed plasmas. The intensities of CF_2, CF_3, and F were measured as a function of pulse phase lags using a time-resolved OES. 300 W of 60 MHz rf power and −900 V of 2 MHz rf voltage were used with the gas flow rates of $C_4F_8/Ar/O_2 = 50/145/5$ sccm and at 26.6 mbar of operating pressure. The pulse duty ratio and the pulse frequency were kept at 50% and 1 kHz, respectively. (a) 60 MHz CW source power/2 MHz CW source power. Both the source power and the bias power were pulsed together with (b) the pulse phase lag of 0°, (c) pulse phase lag of 90°, and (d) pulse phase lag of 180°. (e) is for 60 MHz pulsed source power/2 MHz CW bias power.

without the 2 MHz bias power to the substrate. As shown in Fig. 3(c), possibly due to the low frequency of the 2 MHz bias power which tends to give more power to the incident ions than to the plasma, no significant change in F and CF_x (x = 2,3) (or only slight increases in F and slight decreases in CF_x) were observed during the 0–250 μs compared to the rest of the source power/bias power on-time (250–500 μs). However, as shown in Fig. 3(c), because the 2 MHz bias power was still on during the 500–750 μs, a slower decrease in F density was observed after the initial source power-off. Therefore, the ratios of CF_x(x = 2, 3)/F were lower during the source pulse off-time (500–1000 μs) compared to during the source pulse off-time in Fig. 3(b). When the source power and the bias power were pulsed with the pulse phase lag of 180° as shown in Fig. 3(d), the radicals and ratios of CF_x(x = 2, 3)/F observed during the source power on-time were similar to those observed for the source power on-time (0–500 μs) shown in Fig. 3 (a) and (b). However, when the source power was off (500–1000 μs), the reduction in F density during the source power off-time was the smallest because the 2 MHz bias power was active during the source power off-time. Therefore, the ratio of CF_x(x = 2,3)/F during the source power off-time was also the lowest. As a reference, the radical concentrations of CF_x(x = 2, 3), F, and the ratios of CF_x(x = 2, 3)/F were measured for the condition with only the source power pulsing without the bias power (that is, 60 MHz pulsed source power/2 MHz CW bias power) and the results are shown in Fig. 3(e). As shown, the radical concentrations of CF_x (x = 2, 3) and F and the ratios of CF_x(x = 2, 3)/F were similar to those observed for the condition with the pulse phase lag of 180° shown in Fig. 3(d). These results were observed not only for the source power off-time but also for the source power on-time (or only slight increases in F during the source pulse on-time) possibly due to the low contribution of the 2 MHz bias power to the gas dissociation mentioned above. Therefore, the ratios of CF_x(x = 2, 3)/F measured during the source power off-time was decreased with the increase in pulse phase lag from 0° to 180°.

To understand the gas dissociation characteristics observed in Fig. 3 for the conditions with/without pulsing of the source and bias powers and for the conditions with the different pulse phase lags, the variation of instant electron temperature for the different pulsing conditions was investigated with an emissive probe. To measure the electron temperature with the emissive probe, only Ar was used as the process gas. Except for that, the conditions were similar to the conditions for Fig. 3: that is, 300 W of 60 MHz rf power to the source, -900 V of 2 MHz rf power to the substrate, 26.6 mbar of operating pressure, and 155sccm Ar were used. For the pulsing, 50% of the pulse duty ratio and 1 kHz of pulse frequency were used. In the emissive probe, time varying plasma potentials (V_p) and floating potentials (V_f) were measured and the instant electron temperature (T_e) was calculated from the following equation:

$$V_p - V_f = \frac{kT_e}{2e}\ln\left(\frac{2M}{\pi m}\right)$$

where, k is Boltzmann constant, T_e is the electron temperature, m is the electron mass, and M is the Ar atomic mass. The measured results for different pulse phase lag conditions in Fig. 3 are shown in Fig. 4. The results for the CW power conditions for both the source power and the bias power (that is, 60 MHz CW source power/2 MHz CW bias power) were also included. As shown in the figure, when both the source power and the bias power are in the CW condition, the electron temperature remained at about 7.2 eV. However, when the source power and the bias power were pulsed together with the pulse phase lag of 0°, the exponential decrease of instant electron temperature from 7 eV to about 1 eV after 500 μs was observed due

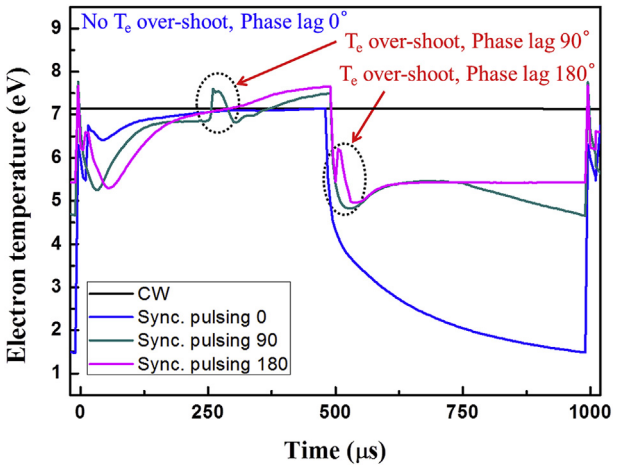

Fig. 4. Instant variation in electron temperature estimated as a function of time for the CW plasma and synchronized pulse phase lag of 0°, 90°, and 180° at the pulse duty percentage of 50% and pulse frequency of 1 kHz. 155sccm of Ar was used as the gas and the other conditions are the same as those in Fig. 3.

to the lack of power application to the source after 500 μs. When the pulse phase lag was 90°, the instant electron temperature decreased from about 7 eV to only about 5 eV until 750 μs. After 750 μs, due to the lack of power application to the source, the instant electron temperature decreased further with time until 1000 μs. When the pulse phase lag was 180°, the instant electron temperature during the source power off-time remained at about 5 eV.

The above results show that, when the source power was on (0–500 μs), the instant electron temperature did not change significantly whether the bias power was on or not due to the higher power input to the plasma by the 60 MHz source power compared to that by the 2 MHz bias power. However, when the source power was turned off (500–1000 μs), the instant electron temperature was significantly dependent on whether the bias power was on or off. The higher the electron temperature, the higher the gas dissociation; therefore, the higher ratios for CF_x(x = 2, 3)/F obtained in Fig. 3 for the decreased pulse phase lag (180° → 0°) appear to be related to the decreased gas dissociation due to reduced bias power to the plasma during the source power pulse off-time (500–1000 μs).

Using the different pulse phase lag conditions investigated in Fig. 3, SiO_2 masked with a 600 nm thick amorphous carbon layer (ACL) was etched and the etch profiles observed by FE-SEM are shown in Fig. 5. The etching conditions are the same as those in Fig. 3. The etch depth of SiO_2 was kept similar at about 1 μm. The etch rates for SiO_2 decreased with increased pulse phase lag, therefore, more etch time was required to etch 1 μm deep SiO_2. In addition, as shown in the figure, as the pulse phase lag became smaller (180° → 0°), the remaining ACL on the SiO_2 became thicker and the SiO_2 etch profile became more anisotropic. The increased anisotropic SiO_2 etch profile, shown in Fig. 5 with the smaller pulse phase lag, appears to be related to the higher fluorocarbon polymer passivation of the sidewall during the source power off-time (500–1000 μs) while etching the SiO_2 with more directional reactive ions during the source power on-time (0–500 μs). During SiO_2 etching masked with ACL, insufficient fluorocarbon polymer passivation results in an increase in the CD of the ACL mask and the ACL mask profile is more sloped due to the increased ACL etching. The increased ACL mask opening increases the top opening CD of SiO_2 etch profile and decreases the bottom opening CD of SiO_2 etch profile, possibly due to the more scattering

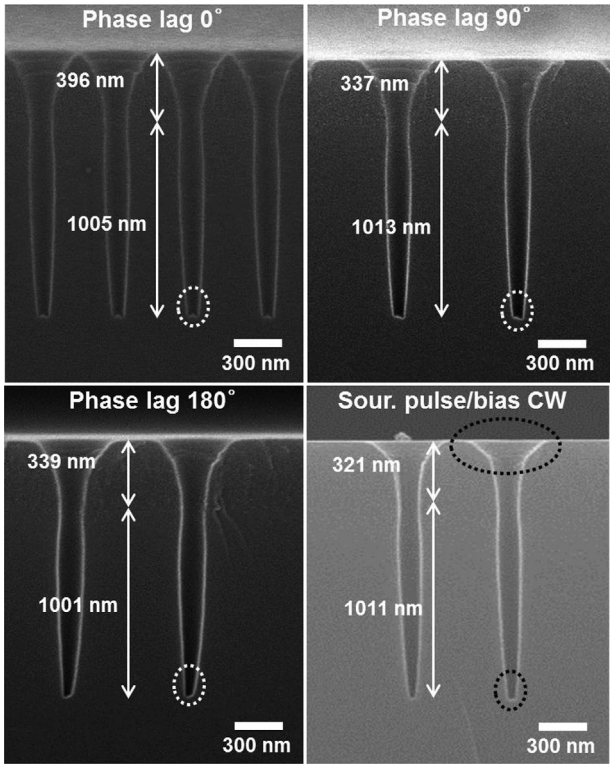

Fig. 5. Etch profiles of ACL masked SiO_2 contact hole pattern observed by FE-SEM after the etching as a function of synchronous pulse phase lag of 0° → 180° with pulse duty percentage of 50% and pulse frequency of 1 kHz. The etch profile for the source power pulsing/CW bias power is also shown. The etch time of SiO_2 contact hole was varied to obtain about 1 μm of etch depth. The process conditions are the same as those in Fig. 3.

of the reactive ions entering the SiO_2 contact hole during the etching. As the pulse phase lag decreased, as shown in Fig. 3, the CF_x(x = 2, 3)/F increased during the source power off-time. Therefore, more fluorocarbon polymer passivation could be obtained during the source power off-time. Consequently, the most anisotropic etch profile was obtained with the pulse phase lag of 0°. In Fig. 5, the SiO_2 etch profile for the source power pulsing/CW bias power is also shown as a reference. As shown in the figure, the remaining ACL thickness was the lowest and the SiO_2 etch profile was the least anisotropic with a sloped bottom area. This may be a result of having the lowest CF_x(x = 2, 3)/F and the lowest fluorocarbon polymer passivation during the source power off-time as shown in Fig. 3(b).

The thickness of the fluorocarbon passivation during the etching for different pulse phase lags was estimated by XPS depth profiling of the etched SiO_2 surface and by measuring the narrow scan data of C1s. The etch conditions are the same as those in Fig. 5. XPS depth profiling data were collected four times (total 120s) after sputtering the etched SiO_2 surface for 30s with an Ar^+ ion gun (3 kV energy and 2 μA ion current). The results are shown in Fig. 6 for the pulse phase lag of 0 and 180°. As a reference, the XPS depth profiling data of C1s for the SiO_2 etching with the source power pulsing/CW bias power are also included. As shown, a thicker fluorocarbon passivation layer was observed for the pulse phase lag of 0° compared to the pulse phase lag of 180°. Also, the SiO_2 surface etched with the pulse source power pulsing/CW bias power, which had the worst SiO_2 etch profile in Fig. 5, had the thinnest fluorocarbon passivation layer. Therefore, the improved SiO_2 etch profile obtained with the lower pulse phase lag (180° → 0°) is believed to be related to the increased fluorocarbon polymer passivation during the source power pulse off-time.

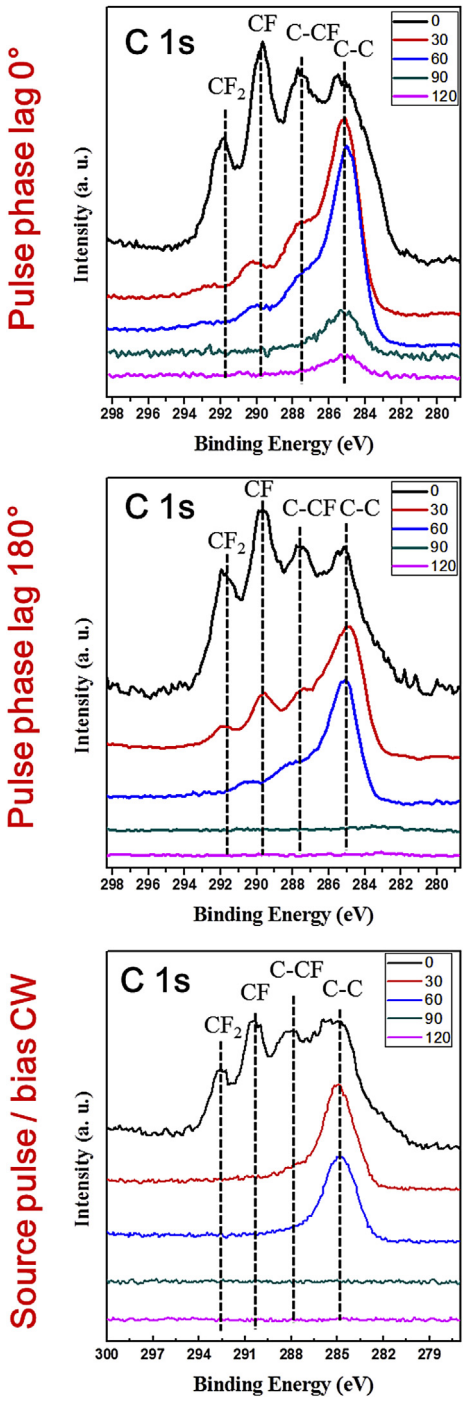

Fig. 6. XPS narrow scan data of C 1s during the depth profiling of the etched SiO_2 surface with the pulse phase lag of 0° and 180° and the source power pulsing/CW bias power pulsing. SiO_2 samples were etched to 1 μm of etch depth in the 60/2 MHz CCP. The process conditions are the same as those in Fig. 3.

4. Conclusions

The effect of pulse phase lag between the 60 MHz source power applied to the top electrode and the 2 MHz bias power applied to the bottom substrate during synchronized dual pulsing with 60/2 MHz CCP on the plasma characteristics and the etch characteristics of SiO_2 was investigated using a $C_4F_8/Ar/O_2$ gas mixture. The concentrations of dissociated radicals such as CF_x (x = 2, 3) and F were related to the source power pulsing rather than the bias

power pulsing. Therefore, during the source power pulse on-time (0–500 μs), the concentrations of CF_x and F did not vary significantly whether the bias power was on or not. However, during the source power off-time (500–1000 μs), gas dissociation by the bias power increased. The ratio of CF_x/F, which is related to the recombination of the dissociated gas, subsequently decreased as the pulse phase lag between the source power pulsing and the bias power pulsing increased from 0° to 180°. Variations in CF_x and F in response to the pulse conditions were related to the change in instant electron temperature measured by an emissive probe. The ratio of CF_x/F was also related to the fluorocarbon polymer passivation during the etching of SiO_2. As the pulse phase lag was reduced from 180° to 0°, the thickness of the fluorocarbon polymer passivation during the etching increased due to the increase in the ratio of CF_x/F during the source power off time. The etch profile of SiO_2 masked with ACL also improved. Therefore, for the synchronized dual pulsed 60/2 MHz CCP, the most anisotropic SiO_2 contact etch profile with the highest SiO_2 etch rate was obtained for the condition with a pulse phase lag of 0° between the source power pulsing and the bias power pulsing.

Acknowledgments

Industrial Strategic Technology Development Program (Development of fundamental technology for 10 nm process semiconductor and 10 G size large area process with high plasma density and VHF condition) funded by the Ministry of Knowledge Economy (10041681, MKE) and also supported by the International Joint Research and Development Program (Large area PECVD equipment development for flexible low temperature high density film deposition) founded by the Ministry of Knowledge Economy (N009300229, MKE).

References

[1] Abe H, Yoneda M, Fujiwara N. Jpn J Appl Phys 2008;47:1435.
[2] Koehler D, Fischer D. ECS Trans 2008;138:47.
[3] Ryu H-K, Lee B-S, Park S-K, Kim I-W, Kim C-K. Electrochem Solid State Lett 2003;6:C126.
[4] Izawa M, Negishi N, Yokogawa K, Momonoi Y. Jpn J Appl Phys 2007;46:7870. Part 1.
[5] Zhang D, Kushner MJ. J Vac Sci Technol A 2001;19:524.
[6] Huang AJJ, Min CC, Ma JK, Tseng YM, Wang WJ, Wu CM, et al. Proc Dry Process Symp 2006:263.
[7] Sakamori S, Maruyama T, Fujiwara N, Miyatake H. Jpn J Appl Phys 1998;37:2321.
[8] Eriguchi K, Ono K. J Phys 2008;D 41:024002.
[9] Kim J, Shin KS, Park WJ, Kim YJ, Kang CJ, Ahn TH, et al. J Vac Sci Technol 2001;A 19:1835.
[10] Hwang GS, Giapis KP. Jpn J Appl Phys 1998;37:2291.
[11] Samukawa S. Appl Phys Lett 1994;64:3398.
[12] Ohmori T, Goto TK, Kitajima T, Makabe T. Appl Phys Lett 2003;83:4637.
[13] Yokozawa A, Ohtake H, Samukawa S. Jpn J Appl Phys 1996;35:2433.
[14] Banna S, Agarwal A, Tokashiki K, Cho H, Rauf S, Lymberopoulos D, et al. IEEE Trans Plasma Sci 2009;37:1730.
[15] Ohtake H, Noguchi K, Samukawa S, Iida H, Sato A, Qian X. J Vac Sci Technol 2000;B 18:2495.
[16] Tokashiki K, Cho H, Banna S, Lee J-Y, Shin K, Moon J-T, et al. Jpn J Appl Phys 2009;48:08HD01.